applied sciences

MDPI

Article

Low-Cycle Reverse Loading Tests of the Continuous Basalt Fiber-Reinforced Polymer Column Filled with Concrete

Jianhang Li [1,2], Hongbo Liu [3,4], Qing Guo [3,4], Guoliang Dai [3,4,*], Junlong Zhou [5] and Penglin Xie [5]

1 School of Transportation and Logistics Engineering, Wuhan University of Technology, Wuhan 430063, China; lijianhangketizu@163.com
2 Jilin Transport Scientific Research Institute, Changchun 130012, China
3 School of Civil Engineering, Southeast University, Nanjing 210096, China; lhb_0803@163.com (H.L.); guoqingah@163.com (Q.G.)
4 Key Laboratory of Concrete and Prestressed Concrete Structure of Ministry of Education, Southeast University, Nanjing 210096, China
5 China Construction Sixth Engineering Bureau Co., Ltd., Tianjin 300171, China; 230169390@seu.edu.cn (J.Z.); daichenchen0520@163.com (P.X.)
* Correspondence: daigl@seu.edu.cn

Abstract: The continuous basalt fiber-reinforced polymer column filled with concrete (BFRPC composite column) can well resist the erosion of the external environment, improve the durability of the structure, and reduce the life-cycle cost of the project. To evaluate the mechanical behaviors of the BFRPC composite column under cyclic lateral loading, laboratory low-cycle reverse loading tests were implemented on a BFRPC composite column specimen, a prestressed reinforced concrete (PRC) tube column specimen, and a prestressed high-strength concrete (PHC) tube column specimen. The failure features, hysteretic curve, and skeleton curve for these three types of column specimens were compared and analyzed through the load–displacement hysteretic curve. The results indicated that the BFRPC composite column possesses the better bearing capacity and deformation performance. The horizontal bearing capacity of the BFRPC composite column is at least three times better than that of PHC and PRC tube columns. Finally, the functional expression of the skeleton curves for the BFRPC composite column is fitted by the rational function fitting method.

Keywords: BFRPC composite column; low-cycle reverse loading test; bearing capacity; failure feature

Citation: Li, J.; Liu, H.; Guo, Q.; Dai, G.; Zhou, J.; Xie, P. Low-Cycle Reverse Loading Tests of the Continuous Basalt Fiber-Reinforced Polymer Column Filled with Concrete. *Appl. Sci.* **2022**, *12*, 6359. https://doi.org/10.3390/app12136359

Academic Editor: Dario De Domenico

Received: 3 May 2022
Accepted: 16 June 2022
Published: 22 June 2022

1. Introduction

Fiber-reinforced composite material is a kind of composite material formed by bonding resin matrix with reinforcing phase continuous fibers such as carbon fiber, glass fiber, aramid fiber, and basalt fiber [1–3]. Compared with traditional building materials such as wood, steel, concrete, etc., fiber-reinforced composite materials have the advantages of high specific strength and specific modulus, excellent fatigue resistance, high fracture safety, and better corrosion resistance [4–6]. Therefore, fiber-reinforced composite materials have unique advantages in foundation engineering.

The mechanical properties of fiber-reinforced composite materials are mainly determined by the type, quantity, and distribution of the fiber [7]. Continuous basalt fiber (CBF) is a new inorganic fiber material [8]. It has the advantages of natural raw materials, high comprehensive performance, low cost, and better compatibility with concrete [9–17]. Compared with continuous fibers such as carbon fiber, glass fiber, and aramid fiber, it has better physical and mechanical properties. Based on the above advantages, CBF materials have been gradually gaining attention in research related to the field of civil engineering such as civil engineering materials and pile and column foundations [18–22].

The mechanical properties of fiber-reinforced polymer columns filled with concrete (FRPC composite column) have been partially investigated by researchers. Yan and

Chouw [23] studied the stress mechanism of FRPC composite columns. The results show that the fiber-reinforced polymer (FRP) tube can significantly improve the ultimate bearing capacity of the specimen. To study the flexural performance of FRPC composite column specimens, Fam and Cole [24] conducted four-point pure bending tests on several groups of different FRPC composite column specimens. The results show that the FRPC composite column specimen has good ductility, significant deformation before failure, and large residual load. Fam and Rizkalla [25] investigated the vertical compressive capacity of FRP tube columns through experimental research and proposed a mechanical model under the action of axial compression. Mirmiran et al. [26] captured from an experimental study that the mechanical properties of FRP columns under hammering are similar to those of prestressed concrete columns. At the same time, many researchers studied the horizontal mechanical behavior of columns with different materials due to the importance of the horizontal bearing capacity for columns. Weaver et al. [27] studied the pile-soil interaction of glass fiber-reinforced polymer (GFRP) tube piles under the action of horizontal bearing capacity through full-scale horizontal bearing capacity experiments. Huang et al. [28] implemented the low cycle pseudo-static tests on four PHC tube column models with various prestress levels to gain insight into their mechanical behaviors. Tang et al. [29] deeply analyzed the mechanical properties of prestressed concrete beams by conducting low-cycle reverse load tests. Murugan et al. [30] conducted low-cycle repeated load tests on six fiber-reinforced polymer tube columns. They studied the horizontal bearing capacity and mechanical properties of carbon fiber-reinforced polymer (CFRP) tube columns and GFRP tube columns, respectively. The results show that the FRP material can significantly improve the horizontal bearing capacity, initial stiffness, and energy dissipation performance of the column. Among them, the improvement effect of CFRP material is better than that of GFRP material.

In general, the existing research on the horizontal bearing capacity of FRPC composite columns mainly focus on fiber-reinforced polymer columns with carbon fiber, glass fiber, and aramid fiber as the reinforcement phase. However, due to the particularities of CBF materials, it is difficult to directly apply the existing research results to the design of tube columns containing CBF materials. Therefore, it is necessary to investigate the horizontal bearing capacity of continuous basalt fiber-reinforced polymer columns filled with concrete (BFRPC composite columns). This work implemented several low-cycle reverse loading tests on a BFRPC composite column specimen, a prestressed reinforced concrete (PRC) tube column specimen, and a prestressed high-strength concrete (PHC) tube column specimen. Then, the phenomena (failure features) and test results (hysteretic curve and skeleton curve) for these three types of column specimens were compared and analyzed. Finally, the functional expression of the skeleton curves for the BFRPC composite column is fitted by the rational function fitting method. The results of this work are expected to provide the technical support and mathematical basis for the horizontal bearing design of BFRPC tube columns.

2. Low-Cycle Reversed Loading Test

The test adopts one BFRPC composite column specimen, one PHC tube column specimen, and one PRC tube column specimen with the same column length and diameter. The point to be explained here is that since the interaction between the surrounding soil and the column is not considered in this study, the column or tube column specimen described herein is essentially a circular or annular section column. In addition, since the cross-sections of the PHC and PRC specimens are the ring, this work terms it as the tube column specimen. The main differences between the three column specimens lie in the contrast in concrete grade and whether the column body is equipped with prestressed steel bar and FRP tube. To investigate the seismic performance of these three columns, such as load-bearing capacity, deformation characteristics, ductility, and energy dissipation, low-cycle reversed loading tests are carried out on these three column specimens, respectively, and their experimental phenomena are discussed and compared.

2.1. Design Parameters of Column Specimens

In this test, the PHC tube column specimen is a standard tube column with concrete grade of C80 (53.6 MPa in the characteristic compressive strength). The PHC tube column specimen is 5 m in column length, 400 mm in diameter, and 95 mm in wall thickness and equipped with seven prestressed main steel bars with the diameter of 10.7 mm. All prestressed steel bars are stretched to 0.7 times their standard tensile strength, that is the tension control ratio of the prestressed steel bars is 0.7. The PHC tube column specimen is made following the national building standards design atlas 10G409 Prestressed Concrete Pipe Piles, prepared by China Institute of Building Standard Design and Research [31].

The parameter and configuration of the PRC tube column specimen are the same as those of the PHC tube pile specimen, except that there are seven other ordinary steel bars with the diameter of 12 mm.

The BFRPC composite column specimen is 5-m long, 400 mm in diameter, 25 mm in wall thickness of FRP tube, and C30 in concrete strength grade (22.6 MPa in the characteristic compressive strength). Four ordinary steel bars with a diameter of 16 mm are arranged along the whole length of the BFRPC composite column specimen, which is symmetrically fixed with stirrups and placed in FRP tube. The FRP tube in the BFRPC composite column specimen is made of the CBF material, and the basic parameters of the CBF material are shown in Table 1.

Table 1. Basic parameters of the CBF material.

Parameter	Single Fiber Diameter	Tensile Strength	Density	Elastic Modulus
Value	17.5 μm	1612 MPa	2.63 g·cm^{-3}	102.9 × 10^3 MPa

The cross-sections of the three kinds of specimens are shown in Figure 1. The basic parameters of the three types of column specimens are summarized in Table 2.

Table 2. Basic parameters of column specimens.

Column Type	Column Length (m)	Diameter (mm)	Wall Thickness (mm)	Type of Steel Bars	Concrete Strength Grade
BFRPC	5	400	25	Ordinary	C30
PHC	5	400	95	Prestressed	C80
PRC	5	400	95	Prestressed and ordinary	C80

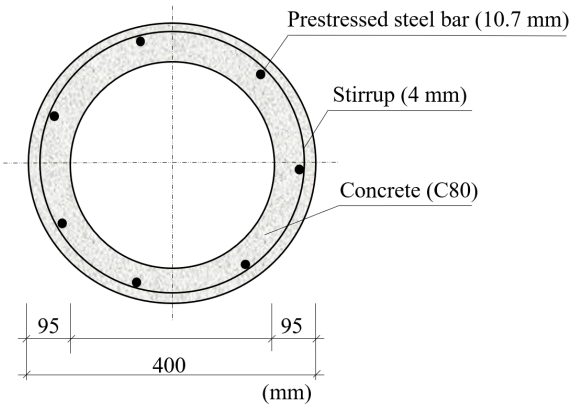

(**a**)

Figure 1. *Cont.*

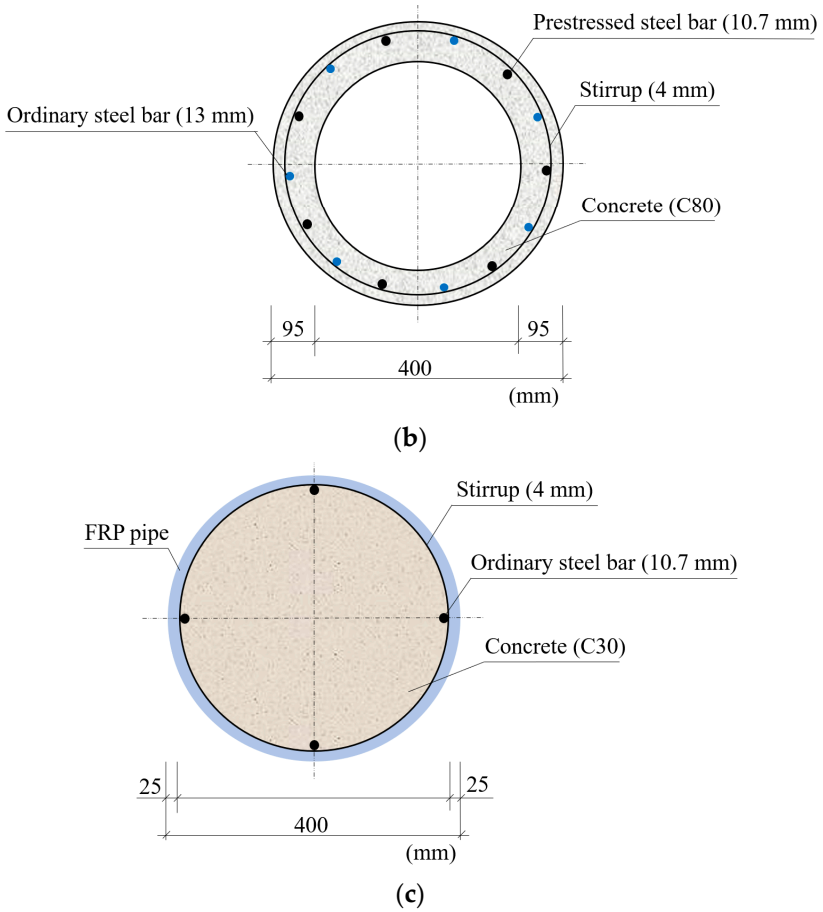

Figure 1. Cross-sections of the three kinds of specimens: (**a**) PHC tube column; (**b**) PRC tube column; (**c**) BFRPC composite column.

2.2. Test Scheme

The test setup mainly includes vertical loading device (comprises the reaction beam and MTS electro-hydraulic servo loading system), displacement meter, pressure bar, arc fixture. Both ends of the column specimen are fixed boundaries. The schematic diagram of the loading device in this test is shown in Figure 2. The assembled field loading device is presented in Figure 3. At the same time, the electric measurement method is used to record the test data.

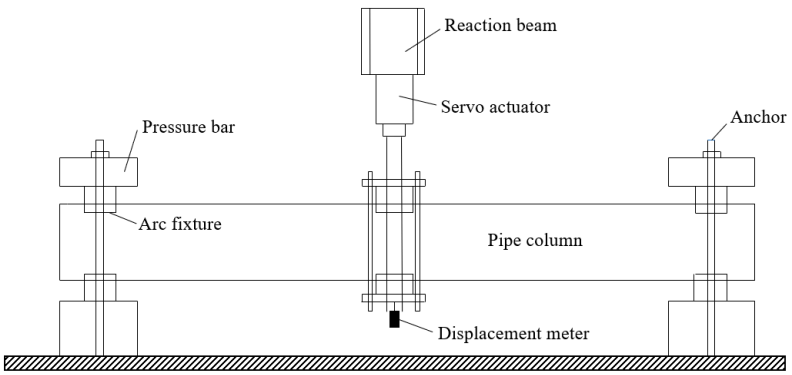

Figure 2. The schematic diagram of the loading device.

Figure 3. The assembled field loading device.

This test adopts the method of load-displacement dual control for the PHC and PRC tube column specimens. Differently, for the BFRPC composite column specimen, since no cracks appear during the test, the displacement-controlled method is directly employed for loading. The load-controlled method increases the load amplitude of each level by 10 kN during the first six levels of loading and by 5 kN thereafter, with one cycle per level and loading speed of 15 kN/min. The displacement-controlled method increases the displacement amplitude of each level by 10 mm during loading, with three cycles per level and loading speed of 5 mm/min. The number of cycles loading and the test termination condition are the same as those of PHC and PRC tube column specimens. The time–history control curve of the cyclic load is presented in Figure 4.

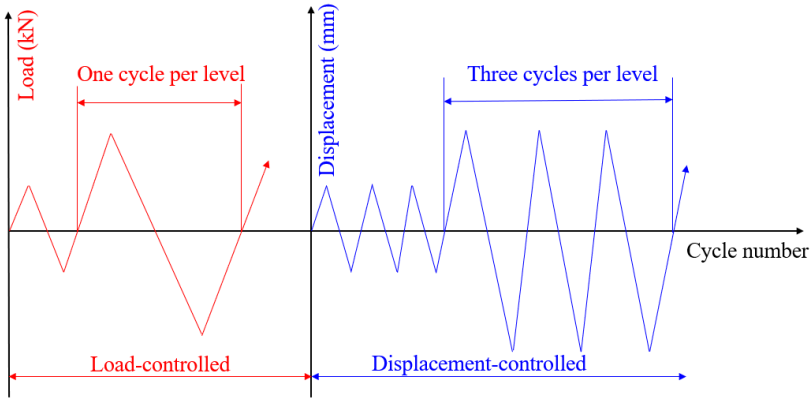

Figure 4. The time–history control curve of cyclic load.

The concrete strain of the column body is measured by concrete strain gauges, and the data are collected by TST3827 data acquisition instrument. To avoid conflict with the position of the arc fixture, strain gauges are attached to the tension and compression sides at a distance of 30 cm from the mid-span of the column along the axis of the column body. The maximum tensile and compressive strain of the bending section for the column specimen can be measured from these two strain gauges. In addition, six strain gauges are arranged uniformly between these two strain gauges to measure the longitudinal strain at different section heights. The specific arrangement of strain gauges is displayed in Figure 5.

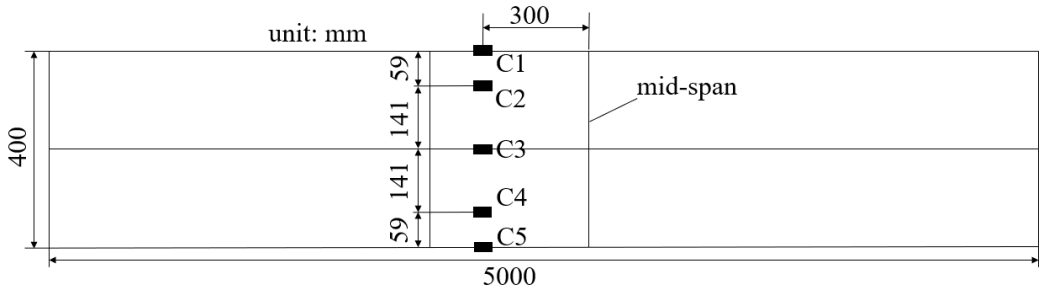

Figure 5. The arrangement of strain gauges.

The MTS electro-hydraulic servo loading system employed in this test can automatically collect the load and deflection values. However, since the arc fixture and the column body cannot be completely fitted, there is a certain gap between them. Therefore, when the load is small, the mid-span deflection of the column body is also slight. It results in a certain error between the displacement automatically collected by the MTS electro-hydraulic servo loading system and the actual displacement of the column body. For this reason, two displacement meters are arranged at the mid-span of the column specimen to monitor the actual mid-span displacement of the column body and correct the data collected from the electro-hydraulic servo actuator.

2.3. Test Results

2.3.1. PRC Tube Column Specimen

Some of the cracks generated in the column specimens during loading are presented in Figure 6. When the forward loading (displacement downward) reached 60 kN, the mid-span displacement of the column specimen was 3.77 mm, and the first crack appeared near the mid-span of the lower part for the column body. When the reverse loading (displacement upward) of 60 kN was applied, the first crack could be completely closed, and no cracks appeared in the upper part of the column body. After that, the loading mode of the displacement-controlled method was adopted. The mid-span displacement of the column specimen formed by the first-level forward displacement loading was 12 mm, and that formed by the first-level reverse displacement loading was −10.68 mm. Under the first-level forward displacement loading, two cracks appeared on the left and right sides of the lower part for the column body, respectively. Under the first-level reverse displacement loading, three cracks appeared on one side of the upper part for the column body, and two cracks appeared on the other side. Moreover, the crack in the lower part of the column body caused by the first-level forward displacement loading extended to the upper part of the column body. After that, 2~3 new cracks were produced in the upper and lower parts of the column specimen under each level of forward and reverse displacement loading, respectively. Among them, the concrete in the mid-span of the column specimen was crushed under the fifth-level forward displacement loading, and the steel bars in the column specimen were fractured during the ninth-level forward displacement loading.

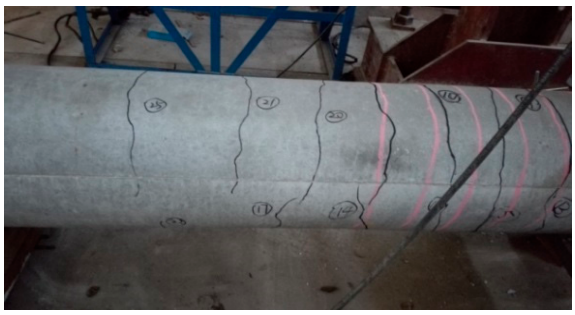

Figure 6. Some of the cracks generated in the PRC tube column specimen during loading.

2.3.2. PHC Tube Column Specimen

The crack development of PHC tube column specimen is presented in Figure 7. When the forward loading reached 75 kN, the mid-span displacement of the column specimen was 4.06 mm, and two cracks appeared near the mid-span of the lower part for the column body. When the reverse loading of 75 kN was applied, these two cracks could be completely closed, and no cracks appeared in the upper part of the column body. After that, the loading mode of the displacement-controlled method was adopted. The mid-span displacement of the column specimen formed by the first-level forward displacement loading was 9.23 mm, and that formed by the first-level reverse displacement loading was −7.52 mm. Under the first-level forward and reverse displacement loadings, one crack appeared on the left and right sides of both the lower and upper parts for the column body, respectively. Moreover, the crack in the lower part of the column body caused by the first-level forward displacement loading extended to the upper part of the column body during the first reverse displacement loading. After that, 1~2 new cracks were produced in the upper and lower parts of the column specimen under each level of forward and reverse displacement loading, respectively. During the third-level forward displacement loading, two steel bars inside the column specimen were fractured, and the other two steel bars were fractured during the third-level reverse displacement loading.

Figure 7. The crack development of PHC tube column specimen during loading.

2.3.3. BFRPC Tube Column Specimen

The BFRPC composite column specimen was loaded directly by the displacement-controlled method. When the forward displacement was loaded to 10 mm, the corresponding load was 70.33 kN, and when the reverse displacement was loaded to 10 mm, the corresponding load was 65.22 kN. No cracks appeared on the surface of the FRP tube for the column specimen during the loading process. At continued displacement loading, the column specimen remained uncracked, but the deformation of the column specimen gradually increased. Moreover, the corresponding load increment decreased at each level of displacement increment; load to the late stage, the column body produced significant deformation. When the forward displacement was loaded to 140 mm, the corresponding load reached 554 kN, and the bearing capacity of the column specimen absented the decreasing trend. However, when the reverse displacement was loaded to 140 mm, the corresponding load reached 592 kN, the FRP tube in the mid-span of the column specimen was split, and the bearing capacity suddenly and significantly decreased. The test phenomenon of the BFRPC composite column specimen is shown in Figure 8.

Figure 8. The test phenomenon of the BFRPC composite column specimen.

2.4. Test Phenomenon Comparison

The first comparison is made in terms of the development of column cracks. The number and distribution of cracks on the concrete surface of the PRC tube column specimen are much larger than those of the PHC tube column specimen. The number of cracks appearing on the surface for the PRC tube column specimen was about 27, while about 12 for the PHC tube column specimen. The farthest crack appearing on the surface for the PRC tube column specimen was about 140 cm from the mid-span, while about 70 cm for the PHC tube column specimen. Differently, The BFRPC composite column specimen is difficult to observe the cracks of internal concrete directly due to the wrapping of continuous basalt fiber. The FRP tube needs to be dissected to observe the crack development in the internal concrete of the column specimen, as shown in Figure 9. The BFRPC composite column specimen formed a crack with the width of 3 cm in the mid-span, and the steel bars were exposed. It indicates that the concrete has completely lost its bearing capacity in the later loading stage. The cracks produced in the BFRPC-combined column specimen show that the FRP tube with the wall thickness of 25 mm can withstand the load even when the steel bar and concrete completely lose their bearing capacity, indicating the excellent mechanical properties of the CBF material.

(**a**) (**b**)

Figure 9. The crack development in the internal concrete of the BFRPC composite column specimen: (**a**) Overall view of cracks; (**b**) crack in the mid-span.

The second comparison is made in terms of the mid-span displacement. The mid-span displacements of PHC and PRC tube column specimens at failure are 23.21 mm and 81.76 mm, respectively, with the bearing capacity of 118.77 kN and 169.59 kN, respectively. The mid-span displacement of the BFRPC composite column specimen at failure is 140 mm, with the bearing capacity of 592.07 kN. It indicates that the configuration of ordinary steel bars can increase the ductility and ultimate bearing capacity of the column to a certain extent, and the employment of the FRP tube will increase that more significantly.

The third comparison is made in terms of the failure mechanism for column specimens. The bearing capacity of the PHC and PRC tube column specimens decreases suddenly due to the fracture of the steel bars. Differently, the bearing capacity of the BFRPC composite

column specimen decreases due to the splitting of the FRP tube in the mid-span. In the initial loading stage, the external loads of all specimens are borne by their column concrete, while the internal steel bars are temporarily unstressed. With load increase, the prestressed steel bars in the PHC and PRC tube column specimens begin to bear the load, while the load of the BFRPC composite column specimen is dissipated by both the ordinary steel bars and FRP tube. With the further increase of load, the prestressed steel bars in the PHC tube column specimen reach the ultimate bearing capacity and break, resulting in the destruction of the column specimen. At this time, the ordinary steel bars in the PRC tube column specimen begin to bear the load together with the prestressed steel bars, and the FRP tube in the BFRPC composite column specimen begins to play a major role in bearing the load. At the end of loading, the steel bars in the PRC tube column specimen break, resulting in the specimen to break and lose its bearing capacity. Although the steel bars in the FPRC composite column specimen yield and the concrete crack, the FRP tube can still bear most of the loads until the mid-span CBF material reaches the ultimate bearing capacity and splits, thus causing the specimen to fail.

3. Analysis of Test Results

This section plots the load–displacement hysteric curves and skeleton curves of the three column specimens on the basis of the data obtained from low-cycle reversed loading tests. Further, the mechanical properties such as bearing capacity, deformation characteristics, and ductility of BFRPC composite column, PHC tube column and PRC tube column specimens are compared. Moreover, the fitting formula of the skeleton curve for the optimal column (BFRPC composite column) is given to facilitate engineering application.

3.1. Hysteric Curves

In the structural seismic performance test, under low-cycle reversed load, a certain residual deformation still exists in the structure or member after complete unloading due to the elastic–plastic characteristics of reinforced concrete structures. A hysteretic loop is formed between the load and the displacement of the column specimen under the action of the forward loading-unloading and the reverse loading-unloading. A series of hysteretic loops are formed under the action of low-cycle reversed loading and thus constitute the hysteretic curve of the specimen. The hysteretic curve is a comprehensive reflection of crack development, steel yielding, concrete breaking, and other phenomena for the column specimen during loading. It is an important tool to analyze the deformation behavior, stiffness degradation, energy dissipation performance, and other mechanical properties of the column specimen. In our test, the load–displacement curves (hysteretic curves) in the mid-span of BFRPC composite column, PHC tube column, and PRC tube column specimen were automatically recorded using the MTS hydraulic servo loading system and corrected by the displacement meter data. The resulting hysteretic curves are demonstrated in Figure 10.

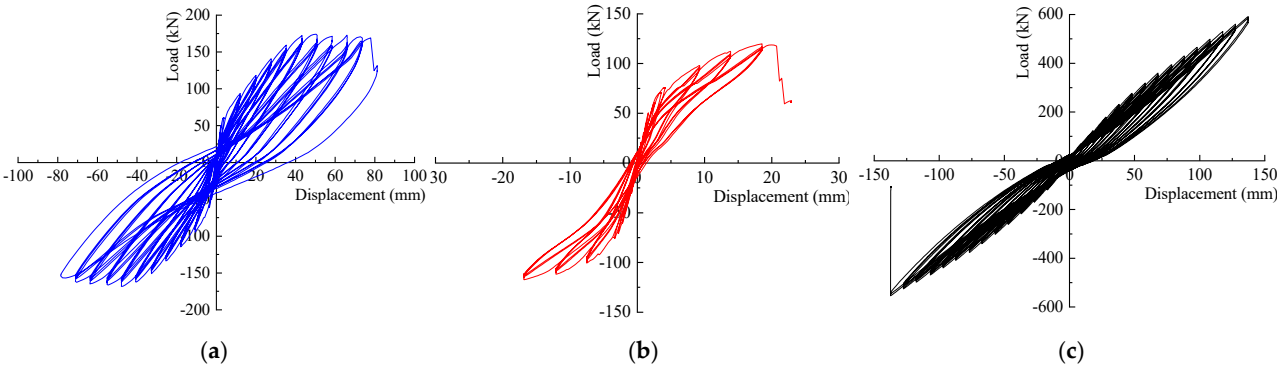

Figure 10. Load–displacement hysteretic curve of each column specimen: (**a**) PRC tube column; (**b**) PHC tube column; (**c**) BFRPC composite column.

The mechanical properties of the BFRPC composite column, PRC tube column, and PHC tube column specimens are compared below in terms of shape, slope variation, and symmetry of the hysteretic curves shown in Figure 10.

From the shape of hysteretic curves displayed in Figure 10a,c, the load–displacement curves of the PRC tube column and the BFRPC composite column specimens are relatively steep at the beginning of unloading, and the displacement recovery is slow. However, with further unloading, the curves tend to be gentle, and the displacement recovery is expedited. In the whole process of low-cycle reversed loading, the accumulations of residual deformation for the BFRPC composite column and the PRC tube column specimens are relatively large, and their hysteretic curves generally present an inverse S-shape. Differently, as illustrated in Figure 10b, the hysteretic curve of the PHC tube column specimen is generally S-shaped, and the accumulation of residual deformation is small. At the beginning of unloading, the load–displacement curve is relatively flat, and the displacement recovery is fast. However, as the load decreases, the load–displacement curve becomes steep, and the displacement recovery slows down. Furthermore, the load–displacement curve of the BFRPC composite column specimen is approximately a straight line during the overall loading process, and the hysteretic curve is not full enough. It reflects the obvious elastic characteristics of the BFRPC composite column specimen during the overall loading process. The hysteretic curves of PRC and PHC tube column specimens are similar to those of the BFRPC composite column specimen at the initial loading stage. The load–displacement curves are approximately a straight line, showing the elastic behavior of PRC and PHC tube column specimens. However, with the increase of the load, the residual deformations of PRC and PHC tube column specimens continue to accumulate, showing apparent plastic behavior for PRC and PHC tube column specimens. Therefore, the hysteretic curves of PRC and PHC tube column specimens are relatively full.

From the slope change of hysteretic curves displayed in Figure 10a,b, the curve slope of PRC and PHC tube column specimens decreases significantly with the increase of load after cracks appear in the column specimens, and the reduction amplitude of the curve slope increases with the increase of load. It reflects the plastic behavior of PRC and PHC tube column specimens. However, the slope of the hysteretic curve for the BFRPC composite column specimen decreases gradually with the increase of load, but the decrease is slight. This indicates that the stiffness degradation of the BFRPC composite column specimen is not obvious, and the bearing capacity is relatively strong.

From the symmetry of hysteretic curves displayed in Figure 10, the forward loading curves of the three column specimens are not entirely symmetrical with the reverse loading curves. The reasons for this result are rough as follows. First, due to the residual deformation in the loading process, it is necessary to overcome the influence of residual deformation in reverse loading. Second, the self-weights of the column body and the fixture make the actual load on the column specimen during the forward loading more significant than that during the reverse loading. Additionally, the asymmetric steel bars of PHC and PRC tube column specimens result in a significant difference between their forward loading curve and reverse loading curve.

3.2. Skeleton Curve

The skeleton curve of the column specimen is formed by connecting the peak points of each stage of the hysteretic curve obtained from the low-cycle reversed loading test. Usually, the shape of the skeleton curve is similar to that of the monotonic loading curve but slightly lower than that of the monotonic loading curve. The skeleton curve reflects the mechanical characteristics of the column specimen in different loading stages, such as stiffness, ductility, and energy dissipation. It is an essential reference for determining the characteristic points of the column specimen, such as cracking load, peak load, and failure load. The skeleton curve of each column specimen and the comparison curve are shown in Figure 11.

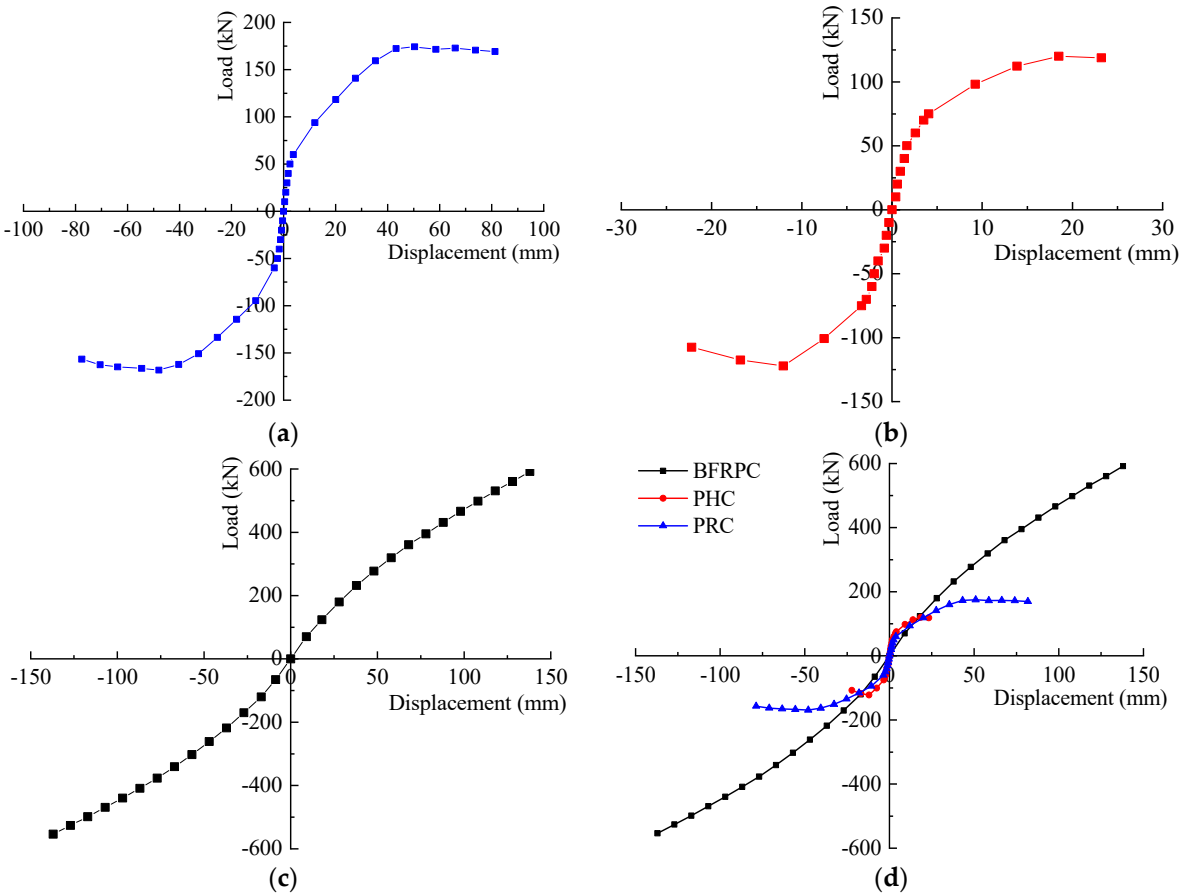

Figure 11. The skeleton curve of each column specimen and the comparison curve: (**a**) PRC tube column; (**b**) PHC tube column; (**c**) BFRPC composite column; (**d**) comparison curve.

The variation of the skeleton curve shown in Figure 11a indicates that the PRC tube column specimen is in the elastic stage before the column concrete cracking, and the change of the specimen stiffness is not significant. Thus, the slope of the skeleton curve remains unchanged. After the column concrete cracks, the slope of the skeleton curve for the PRC tube column specimen decreases significantly, and the skeleton curve tends to be flat. This indicates that the specimen stiffness degrades rapidly. Then, the skeleton curve of the PRC tube column specimen has a longer descending section. When the ultimate load is loaded, the bearing capacity of the PRC tube column specimen falls below 85% of its ultimate bearing capacity, and the column specimen is damaged. As illustrated in Figure 11b, the variation of the skeleton curve for the PHC tube column specimen is similar to that of the PRC tube column specimen, with the difference that the descending section of the skeleton curve is shorter than that of the PRC tube column specimen. The slope of the skeleton curve shown in Figure 11c does not change much overall. This indicates that the BFRPC composite column specimen has significant elastic characteristics during loading and unloading, and the stiffness degradation is slight. The failure of the BFRPC composite column specimen is caused by the sudden drop of the specimen bearing capacity due to the fracture of the FRP tube inside the specimen under the action of the ultimate load. The physical phenomena of the three column specimens displayed in Figure 11 are consistent with the test phenomena stated in Sections 2.3 and 2.4. The feature points of the skeleton curves for the three types of column specimens shown in Figure 11a–c are summarized in Table 3. The cracking point in the table refers to the points where the concrete first cracks, the peak point refers to the points where the load values reach the maximum, and the extreme point refers to the points where the displacement values reach the maximum.

Table 3. The feature points of the skeleton curves.

Column Type	Load (kN) and Displacement (mm)	Forward Loading			Reverse Loading	
		Cracking Point	Peak Point	Extreme Point	Peak Point	Extreme Point
PRC	Load	60	174.96	169.59	−169.14	−156.93
	Displacement	3.77	50.96	81.76	−47.94	−78.74
PHC	Load	75	119.94	118.77	−122.08	−107.44
	Displacement	4.06	18.48	23.21	−12.05	−22.21
BFRPC	Load	/	592.07	592.07	−553.72	−553.72
	Displacement	/	140	140	−140	−140

From the comparative skeleton curves shown in Figure 11d, the skeleton curves of PHC and PRC tube column specimens basically overlap in the elastic phase, indicating that whether the non-prestressed steel bar is configured or not has little effect on the stiffness of the tube column in the early stage of loading. Differently, the slope of the skeleton curve for the BFRPC composite column specimen is smaller than that of the PHC and PRC tube column specimens in the early loading stage but inverse in the later loading stage. This reveals that the stiffness of the BFRPC composite column specimen is smaller than that of the PHC and PRC tube column specimens in the early loading stage, while the stiffness in the later loading stage is more significant than that of the PHC and PRC tube column specimens. Moreover, the ultimate bearing capacity of the PRC tube column specimen (175 kN) is more significant than that of the PHC tube column specimen (120 kN), indicating that the configuration of non-prestressed steel bars can enhance the bearing capacity of the column specimen to a certain extent. The ultimate bearing capacity of the BFRPC composite column specimen is 592 kN, which is much larger than that of the PRC and PHC tube column specimens, indicating that the installation of FRP tube is equivalent to an increase in the reinforcement ratio of the concrete column. Furthermore, the PHC tube column specimen has a short descending section of the skeleton curve before failure, presenting certain brittle failure behaviors. Whereas, the PRC tube column specimen has a long descending section of the skeleton curve before failure, presenting significant ductile failure behaviors. For the BFRPC composite column specimen, the FRP tube made of the CBF material breaks during failure, causing its bearing capacity to drop suddenly, and thus the skeleton curve does not have a descending section due to yielding. However, the BFRPC composite column specimen has large deformation before failure, resulting in significant failure signs. The failure of the BFRPC composite column specimen belongs to ductile failure without yield point, and thus its ductility is significantly less than that of the PRC tube column specimen.

In summary, compared with PRC and PHC tube column specimens, the BFRPC composite column specimen has the better bearing capacity, deformation behavior, and ductility performance. Consequently, to facilitate the wide application of the BFRPC composite column in engineering designs, the functional expression of the skeleton curve obtained from BFRPC composite column test is fitted by the rational function fitting method in this work. The fitting result is exhibited in Figure 12. The functional expression of the skeleton curve is

$$P = \frac{a + b\Delta}{1 + c\Delta + d\Delta^2} \quad (1)$$

where P and Δ stand for the load value and the displacement value, respectively. The coefficients a = 2.66, b = 5.63, $c = -2.89 \times 10^{-4}$, and $d = 1.97 \times 10^{-5}$ with standard errors of 4.49, 0.08, 8.99×10^{-5}, and 8.99×10^{-6}, respectively. The coefficient of determination for the fitting function (R^2) reaches 0.99995, indicating that the fitting value has high accuracy. The functional form of the skeleton curve can be represented by the inverse hyperbolic sine function.

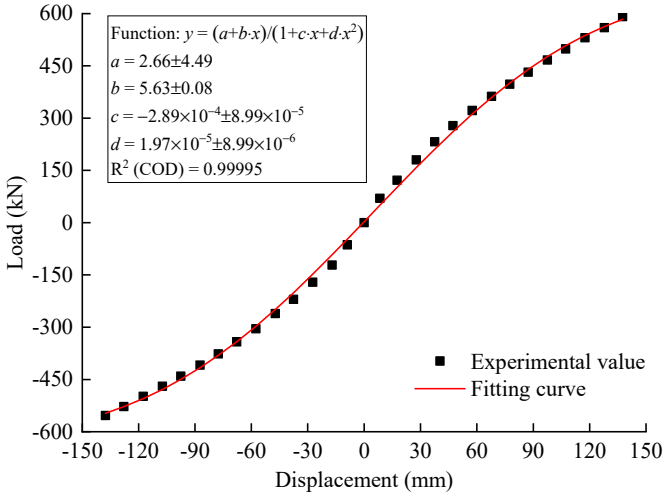

Figure 12. The fitting result of the skeleton curve for the BFRPC composite column.

4. Conclusions

In this work, the load-carrying capacity, deformation characteristic, and ductility performance of the BFRPC composite column under cyclic lateral loading were investigated through comparing with PHC and PRC tube columns. The failure features, hysteretic curve, and skeleton curve for the three columns were compared and analyzed through the load–displacement hysteretic curve. The main conclusions are as follows:

(1) The forward/reverse extreme loads are 118.77 kN/107.44 kN for the PHC tube column specimen, 169.59 kN/156.93 kN for the PRC tube column specimen, and 592.07 kN/553.72 kN for the BFRPC composite column specimen. The forward/reverse extreme displacements are 23.21 mm/22.21 mm for the PHC tube column specimen, 81.76 mm/78.74 mm for the PRC tube column specimen, and 140 mm/140 mm for the BFRPC composite column specimen.

(2) The BFRPC composite column is about 5 times and 6 times than PHC tube column and is about 3.5 times and 2 times than PRC tube column for the horizontal bearing capacity and extreme displacement, respectively.

(3) The failure of the BFRPC composite column belongs to ductile failure without yield point, and its ductility is significantly less than that of PRC tube column. The PHC tube column presents a certain brittle failure behavior.

(4) For the BFRPC composite column the installation of FRP tube is equivalent to an increase in the reinforcement ratio of the concrete column, which can significantly improve its ultimate load carrying capacity.

(5) The functional form for the skeleton curve of BFRPC composite column can be approximately represented by the inverse hyperbolic sine function.

The above results are expected to provide a technical support and mathematical basis for the horizontal bearing design of BFRPC composite columns.

Author Contributions: All authors conceived and designed the study. Conceptualization, methodology, and writing—review and editing: J.L., H.L. and G.D.; writing—original draft preparation and visualization: H.L. and Q.G.; investigation and resources: J.Z. and P.X.; supervision: G.D.; project administration, G.D., J.Z. and P.X. All authors have read and agreed to the published version of the manuscript.

Funding: This research was funded by the Science and Technology Research and Development Project of CSCEC (No. CSCEC-2020-Z-21), and the National Natural Science Foundation of China (NSFC Grant Nos. 52078128, 51878160).

Institutional Review Board Statement: Not applicable.

Informed Consent Statement: Not applicable.

Data Availability Statement: Data are contained within the article.

Conflicts of Interest: The authors declare no conflict of interest.

References

1. Jariwala, H.; Jain, P. A review on mechanical behavior of natural fiber reinforced polymer composites and its applications. *J. Reinf. Plast. Compos.* **2019**, *38*, 441–453. [CrossRef]
2. Ranjbar, N.; Zhang, M. Fiber-reinforced geopolymer composites: A review. *Cem. Concr. Compos.* **2020**, *107*, 103498. [CrossRef]
3. Das, S.C.; Nizam, M.E.H. Applications of fiber reinforced polymer composites (FRP) in civil engineering. *Int. J. Adv. Struct. Geotech. Eng.* **2014**, *3*, 299–309.
4. Gowda, T.G.Y.; Sanjay, M.R.; Bhat, K.S.; Madhu, P.; Senthamaraikannan, P.; Yogesha, B. Polymer matrix-natural fiber composites: An overview. *Cogent Eng.* **2018**, *5*, 1446667. [CrossRef]
5. Dong, Z.; Han, T.; Zhang, B.; Zhu, H.; Wu, G.; Wei, Y.; Zhang, P. A review of the research and application progress of new types of concrete-filled FRP tubular members. *Constr. Build. Mater.* **2021**, *312*, 125353. [CrossRef]
6. Hollaway, L.C. The evolution of and the way forward for advanced polymer composites in the civil infrastructure. *Constr. Build. Mater.* **2003**, *17*, 365–378. [CrossRef]
7. Wang, J.; Gangarao, H.; Liang, R.; Liu, W. Durability and prediction models of fiber-reinforced polymer composites under various environmental conditions: A critical review. *J. Reinf. Plast. Compos.* **2016**, *35*, 179–211. [CrossRef]
8. Jamshaid, H.; Mishra, R.A. green material from rock: Basalt fiber—A review. *J. Text. Inst.* **2016**, *107*, 923–937. [CrossRef]
9. Ivanitskii, S.G.; Gorbachev, G.F. Continuous basalt fibers: Production aspects and simulation of forming processes. I. State of the art in continuous basalt fiber technologies. *Powder Metall. Met. Ceram.* **2011**, *50*, 125–129. [CrossRef]
10. Wang, S.; Zhong, J.; Gu, Y.; Li, G.; Cui, J. Mechanical properties, flame retardancy, and thermal stability of basalt fiber reinforced polypropylene composites. *Polym. Compos.* **2020**, *41*, 4181–4191. [CrossRef]
11. Shi, F.; Su, H.; Zhao, L.; Yu, X.; Li, S. Study on the Structure and Properties of Continuous Basalt Fibres. *Fibres Text. East. Eur.* **2020**, *28*, 52–56.
12. Si, J.; Wang, Z.; Li, J.; Zuo, C.; Zhang, P.; Wei, C.; Wang, J.; Li, W.; Miao, S. Effects of CaO added to raw basalt on producing continuous basalt fibers and their mechanical properties. *J. Non-Cryst. Solids* **2021**, *568*, 120941. [CrossRef]
13. Gutnikov, S.I.; Popov, S.S.; Efremov, V.A.; Ma, P.C.; Lazoryak, B.I. Correlation of phase composition, structure, and mechanical properties of natural basalt continuous fibers. *Nat. Resour. Res.* **2021**, *30*, 1105–1119. [CrossRef]
14. Militký, J.; Kovačič, V.; Rubnerová, J. Influence of thermal treatment on tensile failure of basalt fibers. *Eng. Fract. Mech.* **2002**, *69*, 1025–1033. [CrossRef]
15. Sim, J.; Park, C.; Moon, D.Y. Characteristics of basalt fiber as a strengthening material for concrete structures. *Compos. Part B Eng.* **2005**, *36*, 504–512. [CrossRef]
16. Dias, D.P.; Thaumaturgo, C. Fracture toughness of geopolymeric concretes reinforced with basalt fibers. *Cem. Concr. Compos.* **2005**, *27*, 49–54. [CrossRef]
17. Chiadighikaobi, P.C.; Alaraza, H.A.A.A.; Ibeh, N.U.; Niazmand, M.A.; Adegoke, M.A.; Tefera, B.B.; Vladimir, J.P. Durability assessment of basalt fiber polymer as reinforcement to expanded clay concrete in harsh environment. *Cogent Eng.* **2021**, *8*, 1918855. [CrossRef]
18. Wu, X. Research Progress on Application of Basalt Fiber in Civil Engineering. *Bulletion Chin. Ceram. Soc.* **2020**, *39*, 1043–1056.
19. Zhang, H.; Yao, Y.; Zhu, D.; Mobasher, B.; Huang, L. Tensile mechanical properties of basalt fiber reinforced polymer composite under varying strain rates and temperatures. *Polym. Test.* **2016**, *51*, 29–39. [CrossRef]
20. Sadeghian, P.; Fillmore, B. Strain distribution of basalt FRP-wrapped concrete cylinders. *Case Stud. Constr. Mater.* **2018**, *9*, e00171. [CrossRef]
21. Ding, L.; Liu, X.; Wang, X.; Huang, H.; Wu, Z. Mechanical properties of pultruded basalt fiber-reinforced polymer tube under axial tension and compression. *Constr. Build. Mater.* **2018**, *176*, 629–637. [CrossRef]
22. Suon, S.; Saleem, S.; Pimanmas, A. Compressive behavior of basalt FRP-confined circular and non-circular concrete specimens. *Constr. Build. Mater.* **2019**, *195*, 85–103. [CrossRef]
23. Yan, L.; Chouw, N. Experimental study of flax FRP tube encased coir fibre reinforced concrete composite column. *Constr. Build. Mater.* **2012**, *40*, 1118–1127. [CrossRef]
24. Cole, B.; Fam, A. Flexural Load Testing of Concrete-Filled FRP Tubes with Longitudinal Steel and FRP Rebar. *J. Compos. Constr.* **2006**, *10*, 161–171. [CrossRef]
25. Fam, A.Z.; Rizkalla, S.H. Confinement model for axially loaded concrete confined by circular fiber-reinforced polymer tubes. *Struct. J.* **2001**, *98*, 451–461.
26. Mirmiran, A.; Shao, Y.; Shahawy, M. Analysis and field tests on the performance of composite tubes under pile driving impact. *Compos. Struct.* **2002**, *55*, 127–135. [CrossRef]
27. Weaver, T.J.; Ashford, S.A.; Rollinks, K.M. Lateral load behavior of a concrete-Filled GFRP pipe. In Proceedings of the Geo-Congress 2008 Geosustainability and Geohazard Mitigation, New Orleans, LA, USA, 9–12 March 2008; pp. 931–938.

28. Huang, F.Y.; Wu, S.W.; Luo, X.Y.; Chen, B.C.; Lin, Y.W. Pseudo-static low cycle test on the mechanical behavior of PHC pipe piles with consideration of soil-pile interaction. *Eng. Struct.* **2018**, *171*, 992–1006. [CrossRef]
29. Tang, C.; Ni, J.; Ye, L. Nonlinear Full Range Hysteretic Analysis on Unbonded Partially Prestressed Concrete Beams. *J. Hunan Univ. Nat. Sci.* **2015**, *42*, 62–68.
30. Murugan, M.; Muthukkumaran, K.; Natarajan, C. FRP-strengthened RC piles. II: Piles under cyclic lateral loads. *J. Perform. Constr. Facil.* **2017**, *31*, 04017004. [CrossRef]
31. China Institute of Building Standard Design and Research. Prestressed Concrete Pipe Piles. In *National Building Standards Design Atlas*; China Planning Press: Beijing, China, 2008.